Proceedings of the 29th Annual International
Conference of the IEEE EMBS
Cité Internationale, Lyon, France
August 23-26, 2007.

Enhanced formation of parametric images using fast regressive GLLS for noisy functional imaging

Lingfeng Wen, *Member, IEEE*, Stefan Eberl, *Member, IEEE*, Jing Bai, *Fellow, IEEE* and (David) Dagan Feng, *Fellow, IEEE*

***Abstract*—Parametric images derived in functional imaging can visualize the spatial distribution of physiological parameters *in vivo*. However, the high level of noise intrinsic in single photon emission computed tomography (SPECT) may lead to physiologically meaningless parameter estimates such as negative kinetic rate constants using the generalized linear least squares (GLLS) method for compartmental model fitting. In this study, an enhanced GLLS method using fast regressive adjustment of parameters was investigated for improving the reliability of GLLS applied to dynamic SPECT data. Monte Carlo simulation data were used to systematically evaluate accuracy and reliability of derived parametric images. The simulation and experimental results demonstrate that the enhanced GLLS method can achieve more reliable parametric images, while largely preserving computational efficiency.**

I. Introduction

PARAMETRIC images derived in functional imaging depict the spatial distribution of functional parameters, which are quantitatively related to biochemical or physiological processes *in vivo*. The functional imaging modalities of positron emission tomography (PET) and single photon emission computed tomography (SPECT) are capable of providing parametric images using voxel-by-voxel fitting of tissue time activity curves (TTACs) to an underlying pharmaceutical kinetic model for a given input function (IF) or reference region [1].

The nonlinear least square (NLS) method is regarded as the gold standard for parameter estimation with optimal outcomes. However, it is not well suited to the formation of parametric images as it requires good initial parameter estimates and is associated with marked computational cost. The graphical analysis (GA) methods, such as the Patlak and Logan plots [2, 3], can achieve fast and reliable formation of parametric images using linear regression analysis of transformed data of IF and TTAC. However, the linear plots in the GA methods only provide a limited number of parameter estimates (typically two) and frequently depend on assumptions about the underlying kinetic model, which may not be valid for a given tracer.

The linear least squares (LLS) methods are also fast approaches and estimate parameters from the matrices of linearized equations of the IF and PTAC. The general linear least square (GLLS) method has advanced the LLS method, providing an unbiased, computationally efficient algorithm for full kinetic parameter estimation by introducing an autoregressive filter to address bias due to correlated noise in the measurements [4]. The GLLS method has been successfully applied to PET data to generate parametric images. However, the high level of noise intrinsic in SPECT data can give rise to physiologically meaningless parameter estimates using GLLS such as negative rate constants.

Efforts have been made to improve the reliability of the GLLS method in the formation of parametric images for challenging SPECT data. An integrated method has recently been proposed to combine GLLS with optimal image sampling schedule and cluster analysis [5]. Another approach enhanced the GLLS algorithm's ability to tackle noisy SPECT data using statistical resampling and predefined volumes of distribution, but at the expense of substantially increased computational burden [6].

In this paper, our aim was to enhance GLLS to directly deal with extremely noisy voxel-by-voxel SPECT data, while preserving computational efficiency. An advanced GLLS method using a regressive procedure was investigated with a flexible modeling technique incorporating a new graphical plot, which is referred as the model-aided GLLS. The performance of the enhanced GLLS was evaluated by computer simulations and experimental data for the kinetics of the nicotinic receptor tracer 5-[^{123}I]-iodo-A-85380.

II. Methods

A. GLLS Algorithm

For the three-compartment and four-parameter kinetic model as shown in Fig.1, the tissue time activity function of tracer distribution $C_i(t)$ can be derived from the differential equation in (1) according to the definition of the underlying compartment model.

Manuscript received April 2, 2007. This work was supported in part by ARC, PolyU/UGC, NSFC grants, and ISL/Australia-China special fund.

Lingfeng Wen is with the school of information technologies, University of Sydney and the department of PET and nuclear medicine, Royal Prince Alfred Hospital, Sydney, Australia (phone: +61-2-9515 6170; fax: +61-2-9351 3838; e-mail: wenlf@ ieee.org).

Stefan Eberl is with the department of PET and nuclear medicine, Royal Prince Alfred Hospital, Sydney, Australia and the school of information technologies, University of Sydney, Australia (e-mail: stefan@ it.usyd.edu.au).

Jing Bai is with the department of biomedical engineering, the school of medicine, Tsinghua University, Beijing, China (email: deabj@tsinghua.edu.cn)

(David) Dagan Feng is with School of Information Technologies, University of Sydney, Australia and Department of Electronic and Information Engineering, Hong Kong Polytechnic University, Hong Kong. (e-mail: feng@ it.usyd.edu.au).

$$\frac{d^2}{dt^2}C_i(t) = K_1\frac{d}{dt}C_p(t) + K_1(k_3+k_4)C_p(t) - (k_2+k_3+k_4)\frac{d}{dt}C_i(t) - k_2k_4C_i(t) \quad (1)$$

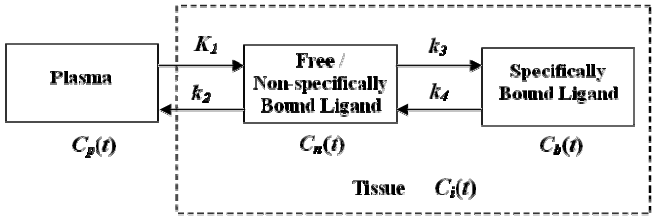

Fig.1 Three-compartment and four-parameter kinetic model for neuroreceptor studies. $C_p(t)$ is the plasma time activity function, which is the input function for the model; $C_i(t)$ is the tissue time activity curve, which is measured by functional imaging.

With the substitutions of $P_1=K_1$, $P_2=K_1(k_2+k_3+k_4)$ $P_3=-(k_2+k_3+k_4)$ and $P_4=-k_2k_4$ in (1), the parameter estimation of GLLS can be obtained in (2) [4].

$$\theta_{GLLS-3comp} = (Z^TZ)^{-1}Z^Tr \quad (2)$$

where $\theta_{GLLS-3comp} = [P_1, P_2, P_3, P_4]^T$,

$$Z = \begin{bmatrix} \psi_1 \otimes C_p(t_1), \psi_2 \otimes C_p(t_1), \psi_1 \otimes C_i(t_1), \psi_2 \otimes C_i(t_1) \\ \psi_1 \otimes C_p(t_2), \psi_2 \otimes C_p(t_2), \psi_1 \otimes C_i(t_2), \psi_2 \otimes C_i(t_2) \\ \vdots \\ \psi_1 \otimes C_p(t_n), \psi_2 \otimes C_p(t_n), \psi_1 \otimes C_i(t_n), \psi_2 \otimes C_i(t_n) \end{bmatrix},$$

$$r = \begin{bmatrix} C_i(t_1) + \hat{P}_3\psi_1 \otimes C_i(t_1) + \hat{P}_4\psi_2 \otimes C_i(t_1) \\ C_i(t_2) + \hat{P}_3\psi_1 \otimes C_i(t_2) + \hat{P}_4\psi_2 \otimes C_i(t_2) \\ \vdots \\ C_i(t_n) + \hat{P}_3\psi_1 \otimes C_i(t_n) + \hat{P}_4\psi_2 \otimes C_i(t_n) \end{bmatrix}.$$ The

values of $\hat{P}_3$ and $\hat{P}_4$ are determined from the previous iteration of GLLS with LLS's results used in first iteration. The values of λ_1 and λ_2 are given by

$\lambda_{1,2} = -(\hat{P}_3 \pm \sqrt{\hat{P}_3 + 4\hat{P}_4})/2$ followed by the definitions of $\psi_1 = \frac{\lambda_2 e^{-\lambda_2 t} - \lambda_1 e^{-\lambda_1 t}}{\lambda_2 - \lambda_1}$ and $\psi_2 = \frac{e^{-\lambda_1 t} - e^{-\lambda_2 t}}{\lambda_2 - \lambda_1}$.

B. Model-aided GLLS

For the challenging voxel-by-voxel curve fitting to SPECT data, visually good fits are usually observed between the measured curve and estimated curve using the original GLLS method. However, good fits do not guarantee that the parameter estimates are physiologically meaningful, which often results in estimates of k_3 and k_4 being negative due to their high sensitivity to noise.

The enhanced GLLS consists of two steps to address the problem. The first step is to estimate partial parameters using the flexible modeling technique. The estimation of K_1 and k_2 for the three-compartment model (Fig.1) are used as the outcomes of the model-aided GLLS.

The volume of distribution (V_d) is a functional parameter of interest to describe the equilibrium distribution of the tracer in the tissue, which is relatively stable compared with other parameters. The estimation of $V_d'=K_1'/k_2'$ for the two-compartment and two-parameter model (Fig.2) can derive an approximate estimation of $V_d=K_1(k_3+k_4)/(k_2k_4)$ for the three-compartment and four-parameter model. The estimation of V_d' is obtained in the first step.

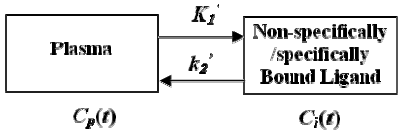

Fig.2 Two-compartment and two-parameter kinetic model.

The second step is to derive estimations of k_3 and k_4 using a new graphical plot with regressive minimization of residual sum of squares (RSSQ) between the measured and estimated curves. The prior information about V_d can derive a linear equation between the estimations of k_3 and k_4 as shown in equation (3) with K_1 and k_2 known for the kinetic model in Fig.1.

$$k_4 = \beta \cdot k_3 = \frac{K_1}{V_d k_2 - K_1}k_3 \quad (3)$$

Substituting k_4 with βk_3 in (1) and integrating the equation will yield estimation of k_3 from the values of K_1, k_2, and V_d, and the IF and PTAC curves and their integral as shown in (4).

$$k_3 = \frac{Y_{k3}}{X_{k3}} \quad (4)$$

where $Y_{k3} = C_i(t) - K_1\int_0^t C_p(\tau)d\tau + k_2\int_0^t C_i(\tau)d\tau$,

$X_{k3}(t) = K_1(1+\beta)\int_0^T\int_0^T C_p(\tau)d\tau^2 - (1+\beta)\int_0^T C_i(\tau)d\tau - k_2\beta\int_0^T\int_0^T C_i(\tau)d\tau^2$.

Plotting X_{k3} vs. Y_{k3} for all the sampling points in the TTAC will derive a line with the slope representing value of k_3 as shown in Fig.3.

However, the estimate of V_d' from the two-compartment model does not necessarily provide an accurate estimation of V_d for the three-compartment model. Thus, a fast iterative procedure is applied to regressively adjust the value of V_d for estimating k_3 by the graphical plot to minimize RSSQ between the measured and estimated TTACs.

For the *i*th estimate of volume of distribution, V_d^i, in the iterative procedure, the estimate of V_d^{i+1} is chosen from $V_d^{i+1}{}_{1,2} = V_d^i \pm 2^{-i}V_d^0$ with the smaller RSSQ value. The

value of V_d^0 is given by an empirical equation from the estimate for the two-compartment model. If the post-iteration RSSQ is not decreased, the iteration was terminated. The derived values of k_3 and k_4 with the minimum RSSQ are used as the output of the second step.

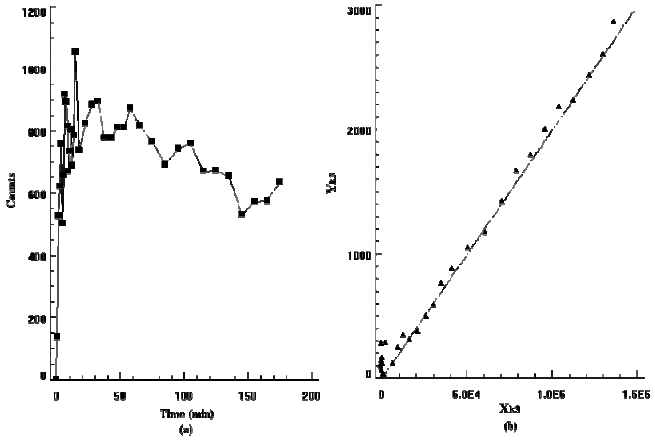

Fig.3 The example of the graphical plot of k_3 for a voxel-wise TTAC. (a) one voxel TTAC, (b) graphical plot for k_3

C. Computer Simulations and experimental data

Computer simulations were performed using the SimSET Monte Carlo code [7] based on a mathematical human brain phantom [8]. Noise-free projection data were generated in accordance with the specifications of a Triad XLT triple head gamma camera (Trionix Research Laboratories, Twinsburg, OH). The dynamic projection data were then generated based on the experimentally observed kinetics of the nicotinic receptor tracer 5-[^{123}I]-iodo-A-85380 [9]. Five different levels of Poisson noise based on experimental noise levels were generated with 20 sets of dynamic data simulated respectively for each noise level. The projection data were reconstructed by the OS-EM iterative method with attenuation and scatter correction [10, 11]. The effect of high-energy photon penetration was also included in the simulation and corrected prior to reconstruction [5].

The parametric images were generated by voxel-by-voxel parameter estimation using the original and model-aided GLLS method. The parameter estimates were regarded as non-physiological when any of the parameter constants (K_1, k_2, k_3 and k_4) were negative or greater than 1. The corresponding parameters of the voxel were then simply set to zero in this investigation.

Volumes of interests (VOI) derived from the phantom were used to generate the average parameters for thalamus, cerebellum and frontal cortex. To evaluate the estimated accuracy and reliability, percentage bias and coefficient of variation (CV) of the parameters of interests (K_1 and V_d) were derived from 20 sets of parameters at each noise level as compared with the reference values (p_0) as shown in (5) and (6).

$$Bias = \frac{1}{M}\left[\sum_{i=1}^{M}\sum_{j=1}^{N}\frac{p_{i,j}-p_o}{N}\right] / p_o \times 100\% \quad (5)$$

$$CV = \frac{1}{p_0}\sqrt{\frac{\sum_{i=1}^{M}(\sum_{j=1}^{N}\frac{p_{i,j}}{N})^2 - M(\sum_{i=1}^{M}\sum_{j=1}^{N}\frac{p_{i,j}}{N})^2}{M-1}} \quad (6)$$

where $p_{i,j}$ is the functional parameter for the *j*th voxel at the *i*th set of data, M is equal to total number of data sets for each noise level, N is the number of voxels in the VOI.

The studied methods were also used to generate parametric images of K_1 and V_d for baboon studies investigating nicotinic receptors [9].

TABLE I
ESTIMATED PERCENTAGE BIAS (CV%) OF PARAMETERS OF INTERESTS

Noise level	1	2	3	4	5
			Cerebellum		
K_1^	-67.6 (2.2)	-72.1 (2.1)	-76.6 (1.9)	-81.0 (2.1)	-85.3 (1.8)
K_1#	-36.8 (1.6)	-39.2 (1.8)	-41.2 (1.9)	-45.2 (2.4)	-47.5 (2.2)
V_d^	-17.0 (23.1)	14.8 (137.4)	-9.2 (40.9)	-20.7 (45.4)	-1.0 (157.8)
V_d#	-14.7 (2.3)	-16.9 (2.9)	-18.8 (2.5)	-23.4 (2.9)	-25.6 (3.0)
			Frontal Cortex		
K_1^	-85.3 (1.1)	-88.1 (0.8)	-90.6 (1.2)	-92.7 (0.8)	-95.0 (0.8)
K_1#	-58.4 (1.3)	-59.8 (1.3)	-61.7 (1.4)	-63.0 (1.2)	-65.2 (1.2)
V_d^	-45.5 (20.5)	-41.1 (37.7)	-46.8 (30.8)	-45.1 (65.9)	-65.5 (19.4)
V_d#	-43.0 (1.8)	-44.3 (1.8)	-46.3 (1.8)	-47.4 (1.6)	-48.6 (2.3)
			Thalamus		
K_1^	-90.5 (1.6)	-91.5 (2.8)	-92.6 (1.8)	-94.1 (2.0)	-95.9 (1.7)
K_1#	-53.5 (5.2)	-54.1 (4.1)	-54.8 (5.6)	-55.5 (4.2)	-55.3 (4.6)
V_d^	-42.5 (56.3)	-34.1 (71.9)	-25.7 (86.9)	-48.8 (55.2)	-74.9 (19.0)
V_d#	-35.6 (7.4)	-36.3 (5.5)	-37.4 (8.4)	-37.7 (6.4)	-36.1 (7.5)

^ ORIGINAL GLLS, # MODEL-AIDED GLLS

III. RESULTS

Table I lists the percentage bias and CV of parameter estimates of K_1 and V_d for the cerebellum, frontal cortex and thalamus from the simulation data.

For the parameter estimates of K_1, the model-aided GLLS achieved less bias in the cerebellum and frontal cortex than the original GLLS with higher reliability (CV<2.5%). Somewhat unexpectedly, the reliability of K_1 by the model-aided GLLS was worse than the original GLLS in the thalamus. This is potential due to the thalamus being a small structure, which suffers from partial volume effects, resulting

in comparatively higher CV of K_1 (about 4.8%). In contrast, a large number of the physiologically meaningless parameter estimates for the original GLLS resulted in negative bias close to -100% with lower CV.

For the parameter estimates of V_d, it is interesting to observe that similar biases were achieved by the original and model-aided GLLS. However, V_d of the original GLLS showed high sensitivity to the simulated noise levels with extremely high CV (exceeding 160%).

Despite of a reduced number of physiologically meaningless fits for the model-aided GLLS, a small number of voxels may still suffer from negative estimates of k_3 from the graphical plot due to severe noise effects. This partially contributed to the high bias of the parameter estimates (> 40%) in the thalamus and frontal cortex. However, the main factor contributing to the bias was the lack of partial volume effect correction in this investigation, resulting in higher bias in the small region like the thalamus and thinner region like the frontal cortex.

The total computational cost of the model-aided GLLS method was about 2.8 times of the original GLLS. The model-aided GLLS does not involve additional computation of the matrix equation (2), unlike the bootstrap Monte Carlo aided GLLS [6]. The iterative process introduced with the graphical plot consists of regression analysis and curve estimation, which only contribute slight computational cost.

Overall, the model-aided GLLS efficiently improved the performance of parameters estimates for noisy SPECT data from the simulation data.

Fig.4 shows the parametric images of K_1 and V_d derived by the studied methods for the experimental data. In contrast to a number of 'black hole' (zero) by the original GLLS in Fig.4(a) and Fig.4(c), the model-aided GLLS clearly provided better parametric images as shown in Fig.4(b) and Fig.4(d).

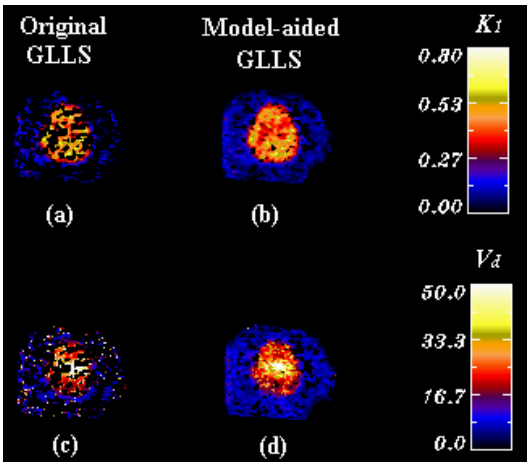

Fig.4 Parametric images of K_1 and V_d for the experimental data (a) K_1 by the original GLLS, (b) K_1 by the model-aided GLLS, (c) V_d by the original GLLS and (d) V_d by the model-aided GLLS.

IV. CONCLUSION

An enhanced GLLS method was investigated to combine a flexible modeling technique and a graphical plot. A fast iterative adjustment was also included to provide physiologically meaningful parameter estimates for noisy functional imaging. The simulation and experimental results show that the enhanced method efficiently improved reliability of GLLS for voxel-by-voxel parameter estimation, while at the same time largely preserving the computational efficiency of the original GLLS. Further investigation such as wavelet filtering is warranted to eliminate the small residual number of physiologically meaningless parameter estimates.

REFERENCES

[1] D. Feng, L. Wen, and S. Eberl, "Techniques for Parametric Imaging," in Biomedical Information Technology, D. Feng, Ed. San Diego: Elsevier press, In press.

[2] C. S. Patlak and R. G. Blasberg, "Graphical Evaluation of Blood-to-Brain Transfer Constants from Multiple-Time Uptake Data. Generalizations," Journal of Cerebral Blood Flow and Metabolism, vol. 5, pp. 584-590, 1985.

[3] J. Logan, J. S. Fowler, N. D. Volkow, et al., "Graphical Analysis of Reversible Radioligand Binding from Time-Activity Measurements Applied to [*N*-^{11}C-methyl]-(-)-Cocaine PET Studies in Human Subjects.," Journal of Cerebral Blood Flow and Metabolism, vol. 10, pp. 740-747, 1990.

[4] D. Feng, S.-C. Huang, Z. Wang, et al., "An Unbiased Parametric Imaging Algorithm for Nonuniformly Sampled Biomedical System Parameter Estimation," IEEE Transactions on Medical Imaging, vol. 15, pp. 512-518, 1996.

[5] L. Wen, S. Eberl, D. Feng, et al., "Fast and Reliable Estimation of Multiple Parametric Images Using an Integrated Method for Dynamic SPECT," IEEE Transactions on Medical Imaging, vol. 26, pp. 179-189, 2007.

[6] L. Wen, S. Eberl, and D. Feng, "Enhanced parameter estimation with GLLS and the Bootstrap Monte Carlo method for dynamic SPECT," presented at 28th Annual International Conference of the IEEE, New York, U.S., 2006.

[7] T. K. Lewellen, R. L. Harrison, and S. Vannoy, "The Simset Program," in Monte Carlo Calculations in Nuclear Medicine, Medical Science Series, M. Liungberg, S. E. Strand, and M. A. King, Eds. Bristol: Institute of Physics Publishing, 1998, pp. 77-92.

[8] I. G. Zubal, C. R. Harrell, E. O. Smith, et al., "Computerized 3-dimensional segmented human anatomy," vol. 21, pp. 299-302, 1994.

[9] M. Kassiou, S. Eberl, S. R. Meikle, et al., "In vivo Imaging of Nicotinic Receptor Upregulation Following Chronic (-)-nicotine Treatment in Baboon Using SPECT," Nuclear Medicine and Biology, vol. 28, pp. 165-175, 2001.

[10] S. R. Meikle, B. F. Hutton, and D. L. Bailey, "A transmission-dependent method for scatter correction in SPECT," Journal of Nuclear Medicine, vol. 35, pp. 360-367, 1994.

[11] H. M. Hudson and R. S. Larkin, "Accelerated image reconstruction using ordered subsets of projection data," vol. 13, pp. 601-609, 1994.